IEEE Access
Multidisciplinary | Rapid Review | Open Access Journal

Received March 4, 2020, accepted March 8, 2020, date of publication March 16, 2020, date of current version March 26, 2020.

Digital Object Identifier 10.1109/ACCESS.2020.2981261

State of Health Monitoring and Remaining Useful Life Prediction of Lithium-Ion Batteries Based on Temporal Convolutional Network

DANHUA ZHOU[1], ZHANYING LI[1], JIALI ZHU[2], HAICHUAN ZHANG[1], AND LIN HOU[1]
[1]School of Information Science and Engineering, Dalian Polytechnic University, Dalian 116034, China
[2]School of Optoelectronic Information and Computer Engineering, University of Shanghai for Science and Technology, Shanghai 200093, China

Corresponding author: Zhanying Li (l_zy1979@126.com)

This work was supported by the National Natural Science Foundation of China under Grant 51337001.

ABSTRACT State of health (SOH) monitoring and remaining useful life (RUL) prediction are the key to ensuring the safe use of lithium-ion batteries. However, the commonly used models are inefficient in predicting accuracy and do not have the ability to capture local regeneration of battery cells. In this paper, a temporal convolutional network (TCN) based SOH monitoring model framework of lithium-ion batteries is proposed. Causal convolution and dilated convolution techniques are used in the model to improve the ability of the model to capture local capacity regeneration, thus improving the overall prediction accuracy of the model. Residual connection and dropout technologies are used to improve the training speed of the model and avoid overfitting in deep network. The empirical mode decomposition (EMD) technology is used to denoise the offline data in RUL prediction, so as to avoid RUL prediction errors caused by local regeneration. The proposed model is verified on two kinds of datasets and the results show that it has the ability to capture local regeneration phenomena in Lithium-ion batteries. Compared with the commonly used models, it has higher accuracy and stronger robustness in SOH monitoring and RUL prediction.

INDEX TERMS Lithium-ion battery, state of health, remaining useful life, local capacity regeneration, temporal convolutional network.

I. INTRODUCTION

As a new type of high energy storage battery, the lithium-ion battery has been widely used in portable electronic devices, electric vehicles and unmanned aerial vehicles due to its fast charging speed, low self-discharge, long life, high energy density and no memory effect [1]. For lithium-ion batteries, safety and reliability are very important in the recycling process. As an important part of the lithium-ion battery management system (BMS), state of health (SOH) essentially reflects the aging and damage of lithium battery. Therefore, effective monitoring directly affects the performance and safety of the system. Secondly, in order to track the aging degree of the battery cell in real time and then get the remaining useful life (RUL) of the battery cell. It is necessary to design a method to predict the SOH and RUL of the battery cell effectively, so as to take measures before the battery cell causes a system failure.

Due to the degradation of chemical components, the performance of lithium-ion batteries will deteriorate with recycling, resulting in the decline of capacity [2]. Therefore, most researches use the degradation of capacity to represent the aging and deterioration degree of lithium-ion batteries in long-term use. However, the capacity of the battery cell cannot be directly measured. There are many factors that affect battery cell aging. In addition to the internal chemistry of the battery cell, the most specific manifestation is the significant increase in the internal resistance and impedance of the battery cell. But accurate measurements of impedance are difficult and expensive, whereas sensor measurements are easy to collect. So a lot of indirect measurements have been used to predict SOH and RUL for lithium-ion batteries. Currently, these methods are grouped into two categories: model-based and data-driven. The model-based methods mainly include the electrochemical model and the equivalent circuit model

The associate editor coordinating the review of this manuscript and approving it for publication was Yu Liu.

[3]–[6]. The electrochemical model can accurately estimate the health state of the battery cell by studying the electrochemical reaction process inside the battery cell, However, the health estimation based on the electrochemical model is difficult to model and difficult to apply in practice. Torai S et al proposed a model for expressing the differential capacity characteristics of the LiFePO4/graphite battery cell for the SOH prediction. This is directly related to the phase transition behavior of active materials [7]. But the model was tested at an experimental temperature of 25 degrees Celsius, without taking temperature into account. Lyu C, *et al.* restructured the parameters of the single particle model to reduce the model parameters that were too complicated to 10. And a series of specially designed current activations are applied to the battery cell during parameter identification to decouple the overvoltage from the measured terminal voltage. The parameter identification method based on activation and response is simplified to fill the gap between electrochemical model and field research [8]. The disadvantages of this approach are also apparent. It does not account for thermal effects, and there is no evidence that it applies to other types of battery cells. In addition to the electrochemical model, the equivalent circuit model has also been studied and improved. Yang J *et al.* proposed a second order equivalent circuit model based on resistance-inductance network. The main purpose is to use inductance to characterize the current when charging at constant voltage so as to capture the dynamic characteristics of the current in constant voltage mode. Then, multiple inductors connected in parallel are used to improve the fidelity of the model. Finally, the nonlinear least squares is used for parameter identification [9]. This model is only implemented on LiFePo4, failing to consider the temperature factor, and there is much room for improvement. In addition to the improvement of the circuit model, parameter identification of impedance and open circuit voltage is also a key technique in the equivalent circuit model. Cui Y *et al.* proposed a non-destructive method to identify the dynamic impedance parameters of equivalent circuits and an open-circuit voltage measurement method based on short, low current pulses to achieve real-time and rapid measurement of open-circuit voltage. Finally, the least square method is used to update the parameters [10]. This is a relatively simple SOH monitoring method, but the accuracy improvement is limited. In a nutshell, the equivalent circuit model simulates the battery cell characteristics by using electronic components to form a circuit. It is less difficult to model than the electrochemical model. This model has strong realizability and strong dynamic response-ability, but the essence of the equivalent circuit is approximate processing, and the parameter deviation of some models will cause larger prediction errors.

From the above description, it can be seen that model-based methods need to build complex mathematical models to achieve certain accuracy. With the popularity of data, data-driven methods can be used to achieve relatively simple prediction on the premise of ensuring accuracy. The data-driven approach includes three main techniques. The first is machine learning techniques, such as neural networks and support vector machines (SVM); the second is statistical techniques, such as Bayesian linear regression and Gaussian Process Regression (GPR); the third is time series technology, such as autoregressive model and so on. Shen S *et al.* took the voltage, current and capacity of the discrete segment as input and deduced the unknown capacity from the local charging cycle through the deep convolutional neural network. Experiments show that this method has higher accuracy than SVM, but the effect of temperature on capacity is ignored [11]. Choi *et al.* compared the voltage factor only with the multi-channel voltage, current, and temperature, proving that the prediction with multi-channel is more accurate [12]. It is worth noting that in addition to improving the prediction accuracy and efficiency, we find that more improvements have been made in health feature extraction in recent years. Yang D *et al.* extracted four features from the charging curve, analyzed the correlation degree with grey correlation, and then predicted with GPR, and improved the model from similarity measure and covariance function design. The model had strong robustness [13]. Guo *et al.* extracted relevant health features from the charging voltage, current, and temperature curves. From the extracted features, 9 features with the highest correlation were selected and dimensionality was reduced through principal component analysis. Finally, relevance vector machine was used as the prediction model. This method is not affected by the discharge conditions and takes into account the influence of temperature. The accuracy is very high, but there is still a lot of room for improvement due to lack of data [14].

In addition to the improvement in feature extraction, many current models fail to capture the phenomenon of local regeneration of lithium-ion battery capacity [15]. This local regeneration phenomenon is explained as the self-charging of the lithium battery. During the battery cell charging and discharging process, side reactions between the electrolyte and the electrode cause the battery's chemical performance to decline. However, when the battery cell is in a resting state, the electrochemical performance will be restored to a certain extent, so a local peak phenomenon will occur to change the trend of the capacity decline curve. In view of this problem Yu *et al.* used empirical mode decomposition (EMD) to decouple local regeneration phenomena and used multi-scale logistic regressive and GPR to monitor SOH. However, such methods were greatly influenced by the starting point [16]. Therefore, Pang *et al.* put forward improvements for this kind of problems, using wavelet decomposition technology to separate the global trend and local regeneration part, and then improve the prediction accuracy through nonlinear autoregressive neural network, and prove that the starting point has little impact [17]. For a single model, there are some problems such as low generalization ability and insufficient precision. Sun *et al.* proposed a hybrid prediction method based on extreme learning machine (ELM) and particle filter (PF). ELM was used to simulate the decreasing trend of battery capacity, and PF was used to update random parameters in

real time. The hybrid model achieves higher accuracy on the dataset than before the model was mixed [18]. In addition, the hybrid prediction model of the serial or parallel connection between long short-term memory (LSTM) network and Convolutional neural network (CNN) models, as well as the hybrid Elman neural network and LSTM network have achieved high accuracy in related fields [19]–[21]. However, when monitoring SOH, these models cannot avoid using techniques such as wavelet decomposition technology to improve the prediction accuracy of local regeneration phenomena. The reason is that the model itself does not have the ability to capture local regeneration phenomenon. Although the hybrid model has improved prediction accuracy, the training speed of the model will decrease. This is also one of the significances of this paper. In summary, the data-driven method does not need to consider the battery's chemical mechanism but needs sufficient data as support. In recent years, most of the improved models are mainly LSTM models and gated recurrent unit (GRU) models that have proven to be excellent in battery cell prediction [22]–[26]. Another significance of this study is to provide new ideas for improvement.

For most deep learning-based sequence prediction tasks, recurrent neural network (RNN) is often the first choice. However, the performance of the convolution architecture is better than RNN in some recent translation and audio synthesis tasks, and in the multivariate sequence classification task, the network architecture based on full-convolution network (FCN) has recently achieved the latest results [27]. In view of the current situation in the filed of battery performance prediction, which is mostly based on RNN and hybrid networks, we use a temporal convolutional network (TCN) model based on causal convolution architecture to predict the SOH and RUL of lithium-ion batteries with capacity as the index, and apply some improvements in convolution architecture in other fields in recent years to the model. After many experiments and analysis, we find that the TCN model has the ability to capture local regeneration phenomenon, and it has higher accuracy and robustness than other baseline models in SOH monitoring and RUL prediction.

The main contribution of the study can be attributed to the following three aspects:

1) In this paper, a TCN network based on convolutional network structure is proposed to realize high-precision SOH monitoring and RUL prediction of lithium batteries.
2) At present, RNN or a variety of traditional model combinations are commonly used to capture local regeneration phenomenon. Considering the effect of local regeneration phenomenon on the overall SOH monitoring, a new method and improved thinking are proposed in this paper, which can solve the problem of battery performance prediction more simply and effectively.
3) Combined with EMD, the global degradation and local regeneration of the battery cell capacity were separated to improve the prediction accuracy of the TCN model for RUL of lithium-ion battery.

The rest of this paper is organized as follows. The dataset of lithium-ion battery is analyzed in Section II. In Section III, we introduce the basic structure of TCN model and the algorithm used in this paper. In Section IV, our model is tested. In Section V, we give the conclusion of the article.

II. CAPACITY DEGRADATION DATASET

A. THE DEFINITION OF SOH AND RUL

Considering that current, voltage and internal resistance are used as the input and data acquisition is complicated and local regeneration is ignored, which leads to low prediction accuracy, this paper directly takes capacity as the prediction target. Before introducing the dataset used, we define the problems that need to be solved. The percentage of available battery cell capacity is defined as SOH in this study, and the formula is as follows:

$$SOH\ (t) = \frac{C_t}{C_o} \tag{1}$$

In (1), C_o represents the initial capacity, C_t represents the capacity of the t-th cycle, and the ratio of the two represents the current SOH value. The problem that we need to solve is to predict the value of SOH in the next step through a series of already obtained SOH values. The definition of battery RUL is as follows:

$$RUL\ (t) = t - t_{EOL} \tag{2}$$

In (2), t_{EOL} means end-of-life (EOL) is the number of cycles at the end of battery life, and t is the t-th cycle number. Get the current battery's RUL from the difference between the current capacity and the EOL. The problem that we need to solve is to realize multi-step prediction of RUL through offline data [28].

B. DATASET

Two public lithium-ion battery datasets are used in this study, one from the NASA Ames Prognostics Center of Excellence (PCOE) [29]. The battery cell has a rated capacity of 2.0Ah. Cyclic charge and discharge at room temperature of 24 degrees Celsius. Take battery numbers B0005, B0006, and B0018 as examples. In 1.5A constant current charging mode until the voltage reaches 4.2V, then constant voltage charging until the current drops to 20mA. Discharge conditions are constant current 2A discharge until the voltage drops to 2.7V, 2.5V and 2.2V respectively. Another dataset from the Center for Advanced Life Cycle Engineering (CALCE) at the University of Maryland [30]. The battery cell has a rated capacity of 1.1Ah. Similarly, the charging method of constant current first and constant voltage later is selected, but different discharge currents are selected. Three battery cells with different discharge modes are selected to verify the performance of the model. Details of the selected lithium-ion batteries are in Table 1. Through accurate prediction of these commonly used batteries, it is proved that our model can accurately predict other unknown batteries with merely a small amount of capacity training data.

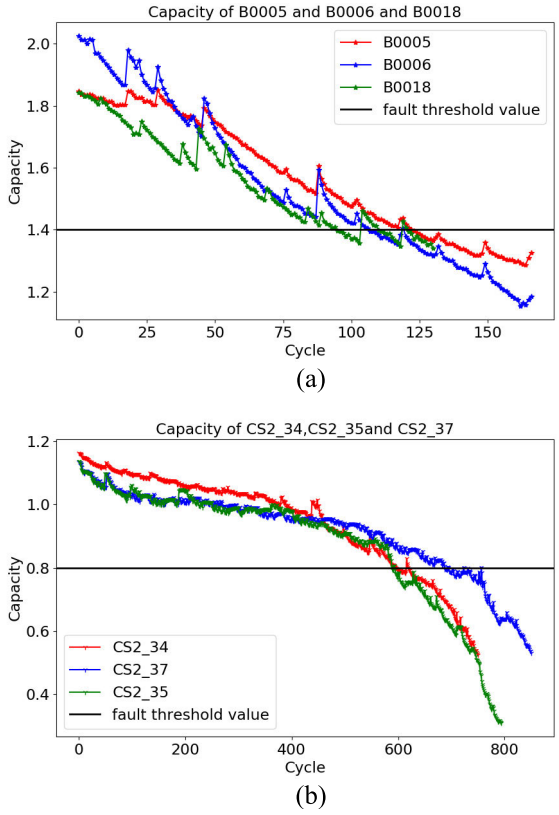

FIGURE 1. Lithium ion battery capacity degradation curve. (a) NASA dataset. (b) CALCE dataset.

TABLE 1. Test lithium-ion batteries information.

Battery ID	Discharge current	Rated capacity	CC/CV	End voltage
B0005	2A	2Ahr	1.5A/20mA	2.7V
B0006	2A	2Ahr	1.5A/20mA	2.5V
B0018	2A	2Ahr	1.5A/20mA	2.5V
CS2_34	0.5C	1.1Ahr	0.5C/0.05A	2.7V
CS2_35	0.5C	1.1Ah	0.5C/0.05A	2.7V
CS2_37	1C	1.1Ahr	0.5C/0.05A	2.7V

Generally speaking, in order to ensure the safety performance of the system, the life limit is to reduce the capacity to 70% - 80% of the nominal capacity [31]. NASA's dataset defines 30% of rated capacity as EOL, or 1.4Ah. The attenuation curve of battery capacity is shown in Figure. 1(a). The dataset of CACLE usually defines 20% of the rated capacity as EOL. In this paper, 0.8Ah is taken, and the battery cell capacity attenuation curve is shown in Figure. 1(b).

Figure 1 shows that the battery cell capacity decay paths are very similar at the same discharge rate. Different discharge rates differ significantly on the decay path, and this difference is precisely due to various uncertain factors of battery aging. In systems with a large number of lithium-ion batteries such as electric vehicles, inconsistent battery performance can seriously affect the safety performance of the system. This illustrates the importance of effective SOH monitoring and RUL prediction for lithium-ion batteries. We will also find that there is local capacity regeneration phenomenon for different lithium-ion battery capacity sequences. This is the common feature of battery capacity sequences, so it is important to improve the model's ability to capture local capacity regeneration phenomenon under different battery cells and different operating conditions. This is also the key to improving the accurate monitoring of SOH by the model.

In Figure 1, under different operating conditions, the capacity attenuation slope of the battery at EOL is also different, which means that our model must have the ability to predict long-term in order to achieve high accuracy in RUL prediction. And the local regeneration phenomenon in Figure 1 will also affect the accurate positioning of EOL, and the prediction result of RUL highly depends on the accurate prediction of battery EOL, so it is necessary to preprocess the offline data during RUL prediction. The purpose of preprocessing is to reduce the impact of local fluctuations on model prediction. This is a way to improve the accuracy of the model in terms of RUL prediction.

III. MODEL ARCHITECTURE AND ALGORITHMS

In recent years, some convolutional architectures can achieve the highest accuracy in audio synthesis, machine translation, and language modelling [32]. Considering that the capacity sequence is a small sample, combined with the best practices of modern CNN architecture in other fields, the TCN structure selected in this paper is simpler and easier to implement than Wavenet [33]. It removes the gate mechanism and adds a residual system. The TCN model used has the following characteristics:

1) Using causal convolution and dilated convolution so that historical information will not be missed, thus the prediction of local regeneration phenomena is more stable.
2) Similar to the RNN model, the TCN model uses one-dimensional FCN to accept input sequences of any length and map them to output sequences of equal length. However, compared with the RNN architecture of the same capacity, the TCN model parameters are shared, so the training memory is lower.
3) CNN model uses the same convolution kernel at each layer, so, the TCN model can process long sequences in parallel.
4) Unlike the periodic structure, the propagation path of the TCN model is independent of the time direction, so there is no gradient explosion.

A. DILATED CONVOLUTION

Using the causal convolution model to consider all the historical capacity sequence information will inevitably lead to the deepening of the network. The principle is shown in Figure 2. To solve the problems of training speed and memory caused by network depth, two solutions are proposed. The first is a dilated convolution technique [34], and the other is a skip connection technique. Dilated convolution was first

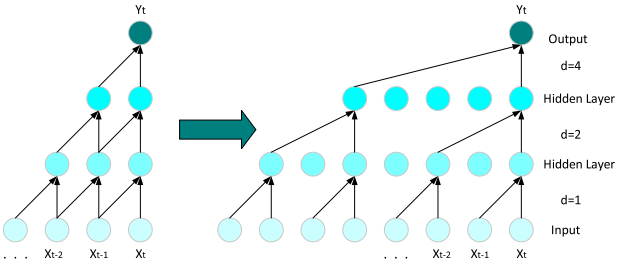

FIGURE 2. Visualization of dilated convolution.

proposed to solve the problem of information loss in semantic segmentation of images. In the original image segmentation, the pooling layer was used to reduce the image size and increase the receptive field to represent a large range of input better, and then upsampling to expand the image size. The problem of information loss during this period is solved by not doing the operation of downsampling. However, only increasing the number of convolutional layers will increase the calculation amount of the network, and no pooling will be done to aggregate the features, so the final effect of feature extraction will be affected. The essence of the problem is that the receptive field cannot be changed, so the dilated convolution operation is proposed. In fact, setting the step size for common convolution operations greater than 1 will also increase the receptive field, but there is a problem of reducing the image size. Therefore, dilated convolution is a major improvement on CNN.

At present, two problems need to be solved for dilated convolution. The first is that the filter with the same dilation factor will have a 'gridding effect' after multiple iterations; that is, the continuity of information is lost. Missing information leads to sparse input, which is fatal for sequence prediction tasks. The second problem is the size of the value of dilation factor, because the larger dilation factor in the image only works better for larger objects, and it is harmful to smaller objects. Similarly, for capacity sequences, appropriate dilation factor will affect the accuracy of local fluctuation prediction. To solve the 'gridding effect', the article uses hybrid dilated convolution (HDC) [35]. HDC is an improvement proposed in [36] and [31] that the value of d should be of the form (e.g., 2, 4, 6). The structural design for the dilation factor is $d = [r_1, r_2, \ldots, r_i, \ldots, r_n]$, the filter is $k \times 1$, and dilation factor needs to meet the following conditions:

1) The convolution dilation factor cannot have a common divisor greater than 1; otherwise, the 'gridding effect' will still appear at the top of the network, which is the key difference from [36] and [34].
2) Design the dilation factor into a zigzag shape to take into account the information of different distances, such as: [1, 2, 5].
3) The formula that defines the maximum distance between two non-zero values in the filter is:

$$M_i = \max\left[M_{i+1} - 2r_i, M_{i+1} - 2\left(M_{i+1} - r_i\right), r_i\right] \quad (3)$$

At layer n, $M_n = r_n$, our goal is $M_2 \leq k$. An example that does not meet the requirements is $d = [1, 2, 9]$, When $k = 3, M_2 = 5$ is larger than 3. The purpose of this requirement is to at least cover all the information with a dilation rate equal to 1, thereby ensuring that no information leakage occurs. This is the key to ensuring that our model is more sensitive to local regeneration, thus improving its ability to capture local regeneration. We explain the variation of the causal convolution plus the dilation convolution in Figure 2.

The formula for the expansion convolution of the one-dimensional volume sequence used in the article is as follows:

$$F(i) = \sum_{k=1}^{K} f\left(i + d \cdot k\right) \cdot h(k) \quad (4)$$

In (4), i represents the ith element in the sequence. K is the maximum value of k, which represents the size of the filter. $f(i)$ is a one-dimensional input sequence, $F(i)$ is an output sequence, $h(k)$ is a filter of length K, and d is a dilation factor. For a convolution kernel of size $k \times 1$, the value of the dilated filter obtained by inserting a numeric zero operation is $k_d \times 1$.

$$k_d = k + (k - 1) \cdot (d - 1) \quad (5)$$

B. RESIDUAL BLOCK

To some extent, deep neural networks will have better expressive ability and predictive performance. The use of skip connections is the second way to solve the problems caused by the depth of the network. This is also the key to our model's ability not only to capture local regeneration but also to be faster than commonly used hybrid models. The skip connection originates from the residual network (ResNet) [37]. Its essence is a new idea and not a new formula, which aims to solve the problem of network degradation and gradient disappearance. If the model takes x as the input value, and $F(x)$ is the output after a linear transformation and activation, then before the linear transformation on the second layer is activated, $F(x)$ is added to the input x of the previous layer, and then the output O is activated. The specific formula is as follows:

$$O = Activation\left(x + F\left(x\right)\right) \quad (6)$$

Then such a connection process is a skip connection, and each connection constitutes a residual block, and a plurality of residual blocks connected together is a ResNet. We design the residual block, as shown in Figure 3 based on the characteristics of the capacity sequence data. The residual block consists of two layers of dilated causal convolution, with ReLU as the activation function and dropout technique to prevent overfitting [38]. We also introduced an optional 1×1 convolution to ensure that the input and output of the residual block have the same widths. To make our technique look simpler, we use the same type of legend to explain the improvement process at each step of our model. The process of adding skip connections based on the causal convolution model is shown in figure 4. In figure 5, we use the same type

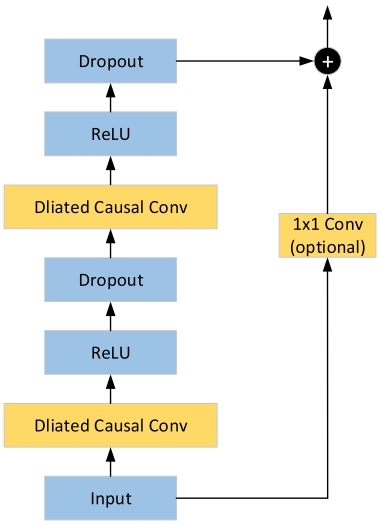

FIGURE 3. Visualization of residual block.

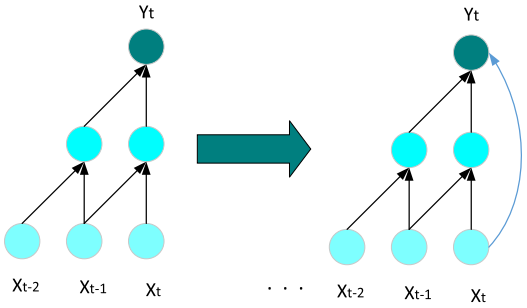

FIGURE 4. Skip connection flowchart.

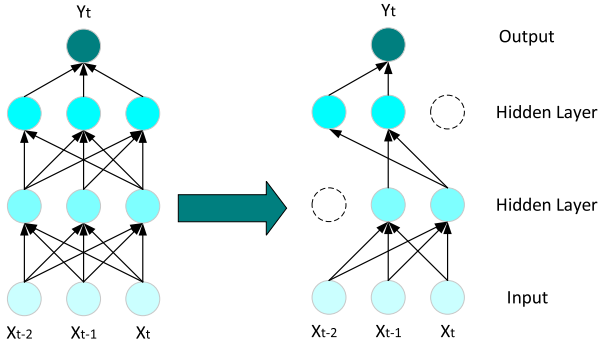

FIGURE 5. Dropout technical flowchart.

to show the changes we made to the model using dropout technology.

C. EMPIRICAL MODE DECOMPOSITION

EMD is a mathematical time domain decomposition method proposed for analyzing non-stationary and nonlinear signals in 1998 [39]. Compared with wavelet decomposition and Fourier transform, EMD is adaptive based on the time scale of the signal. EMD can decompose a complex time series into a series of signals with local characteristics, that is, intrinsic mode functions (imf) and corresponding residual values (res). Each of the decomposed imfs contains local characteristics of different time scales of the original time series, and the global decay and local regeneration of the battery capacity sequence should be at different scales. It is reasonable to consider it as a multi-scale mixed signal and to process it with EMD. Each imf of EMD should meet the following conditions:

1) The number of zero-crossing and local extreme points must be equal, or at most differ by 1 in the entire time range.
2) At any point in time, the average of the local maximum envelope and the minimum local envelope must be 0.

The process of EMD decomposition based on this condition is as follows:

1) Find the local extreme values of the original time series $X(t)$, and then use cubic spline interpolation to obtain the upper envelope sequence value $X_{\max}(t)$ of the original time sequence $X(t)$, which is the maximum value line and the lower envelope sequence value $X_{\min}(t)$, which is the minimum value line.
2) Find the instantaneous average value of the upper and lower envelope sequences at each moment, that is, $m(t)$:
$$m(t) = \frac{m_{\max}(t) + m_{\min}(t)}{2} \tag{7}$$
3) Subtract the instantaneous average value m(t) from the original time series $X(t)$ to obtain a new series $h(t)$:
$$h(t) = X(t) - m(t) \tag{8}$$
If the number of extreme points and zero-crossing points of the new sequence h(t) is equal or at most one difference, then h(t) is the imf component. Otherwise, the above steps are repeated until the condition of the imf is obtained.
4) Subtract $imf_1(t)$ from the original sequence after finding the first natural modal function $imf_1(t)$ to get the remaining sequence $r_1(t)$:
$$r_1(t) = X(t) - imf_1(t) \tag{9}$$
5) Then repeat the above steps with $r_1(t)$ as the new original sequence, and extract the nth $imf_n(t)$ in sequence. In the end, $r_n(t)$ becomes a monotonic sequence.

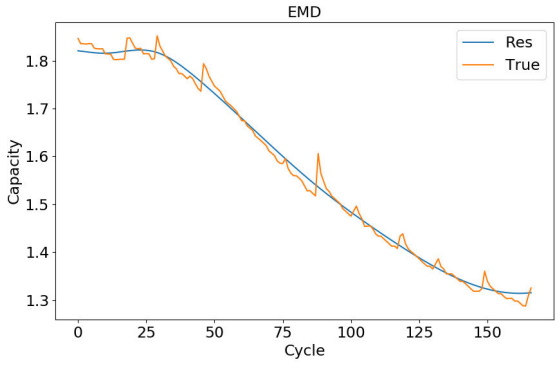

FIGURE 6. Res of B0005.

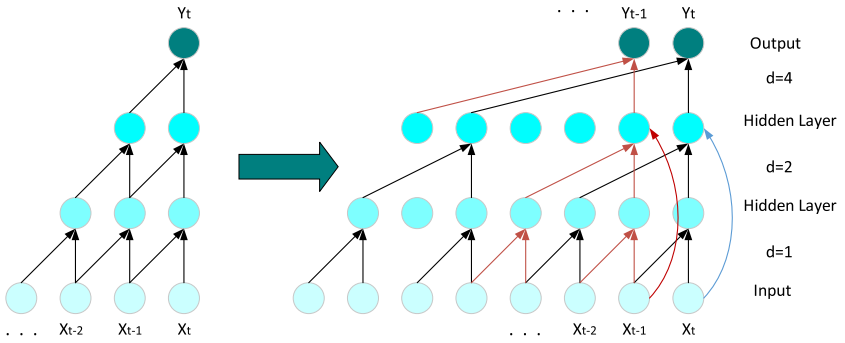

FIGURE 7. Visualization of TCN model.

6) The original sequence $X(t)$ can be obtained by superposing the components after decomposition.

$$X(t) = \sum_{k=1}^{n} imf_k(t) + r(t) \tag{10}$$

Taking the B0005 battery cell used in the article as an example. The original capacity sequence of battery cell B0005 and the res extracted by EMD are shown in Figure 6. From the figure, we can see that res fits the overall downward trend well and effectively removes local fluctuations. Therefore, using res instead of the real value is more suitable to capture the overall degradation trend of the battery. In general, res can reflect the true degradation trend of the battery, avoiding the interference of local fluctuations on the RUL prediction, and can improve the accuracy of the RUL prediction. At present, in the field of battery cell performance prediction, EMD is usually combined with hybrid model to improve the prediction accuracy of lithium battery SOH, but the training speed of this method is very slow. To highlight the superiority of our model over these hybrid models. We also did not use CEEMDAN [40], an improved EMD technology. First, there is no research on whether improved techniques like CEEMDAN can improve the prediction accuracy of RUL. Most of the current studies only show that the correlation with the capacity curve can be improved, and this increase is small for the capacity curve. Secondly, we found through the experiment that when we used EMD technology to decompose the capacity curve into three imfs and res, we set the parameter max_imf=3 for our experiment. At this point, it can be found from the Pearson correlation comparison in table 2 that EMD can obtain a higher correlation than CEEMDAN [26]. Therefore, we use EMD as a de-noising tool for RUL prediction, and its adaptive decomposition can not only remove local regeneration phenomenon, but also be more consistent with the simplicity and high efficiency of our model compared with other complex decomposition technologies.

D. EVALUATION INDEX

To verify the performance of the model in SOH monitoring and RUL prediction, this paper uses root mean squared error (RMSE), mean absolute error (MAE), and RUL absolute error to show that the TCN model has better prediction performance than other models:

TABLE 2. Pearson correlation between EMD and CEEMDAN.

Residual	B0005	B0006	B0018
EMD	0.9969	0.9928	0.9877
CEEMDAN	0.9932	0.9915	0.9799

$$RMSE = \sqrt{\frac{1}{n}\sum_{i=1}^{n}(y_i - \hat{y}_i)^2} \tag{11}$$

$$MAE = \frac{1}{n}\sum_{i=1}^{n}\left|\left(y_i - \hat{y}_i\right)\right| \tag{12}$$

$$RUL_{Error} = \left|RUL_{True} - RUL_{prediction}\right| \tag{13}$$

In (11) and (12), y_i represents the true value of the capacity series, and $\hat{y}_i$ represents the predicted value of the capacity series. RMSE is used to measure the deviation between the predicted value and the true value. MAE can better reflect the actual situation of the predicted value error. The smaller the two, the higher the prediction accuracy. In (13), RUL_{True} is the real RUL, $RUL_{prediction}$ is the predicted RUL, and RUL_{Error} is the absolute error between the two. The smaller the absolute error, the more accurate the model is in predicting the RUL.

E. INTRODUCTION TO THE OVERALL PREDICTION PROCESS

In this section we mainly introduce the algorithms used. The overall framework of lithium-ion battery health prediction combined with all algorithms is given in Figure 8, and the improvement process of the TCN model we used is shown in figure 7. When battery cell capacity data are available, we can take the acquired battery capacity as input to the network. On the basis of one-dimensional causal convolution network, the dilated convolution, residual connection, and dropout technology are added to form the TCN model used in this paper. The TCN model is used as the core to capture the local regeneration phenomenon, thereby achieving

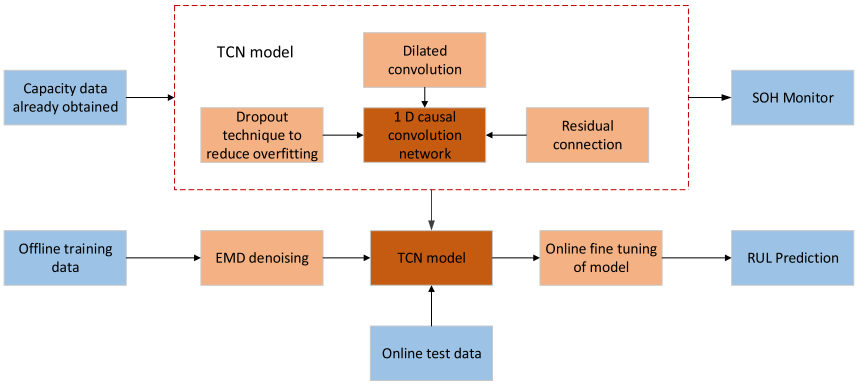

FIGURE 8. System framework for battery health prognostics.

high-precision SOH monitoring. At the same time, EMD technology is used to perform noise reduction processing on offline data, which can also perform effective RUL prediction on online data.

IV. RESULTS AND DISCUSSION

The article mainly verifies the reliability of the model from the following aspects:

1) Compare the effects of different model structures and parameters on the prediction results, and choose the structure that is most suitable for the capacity series prediction in this paper.
2) Verify the performance of TCN model in SOH monitoring and local regeneration phenomenon capturing compared with existing baseline models.
3) Verify the performance of the TCN model in terms of RUL prediction with offline data compared to the baseline model.
4) Verify the reliability of the model on different batteries under different discharge conditions.

The monitoring of SOH in the experiment is mainly to maintain the battery in advance. Therefore, choosing the starting point according to the actual use situation can better explain the reliability of the model. The prediction of RUL is more inclined to replace the battery in practice, so an accurate prediction of the failure point is more important. The experimental analysis models in this article are written in Python 3.6, and the experiments are run on a laptop. The computer configuration is as follows: the CPU is i5-7300, and the GPU is NIVIDA 1050Ti.

A. MODEL STRUCTURE ANALYSIS

The model parameters and structure are experimentally analyzed based on the capacity series data used in the article. Monitor the SOH of the battery from the 60th cycle of battery B0005. That indicates the first 60 cycles are known as the training set, and the rest are known as the prediction set. We use a mechanism similar to sliding window to continuously add the predicted new values into the window, and predict the next SOH value through a series of obtained SOH

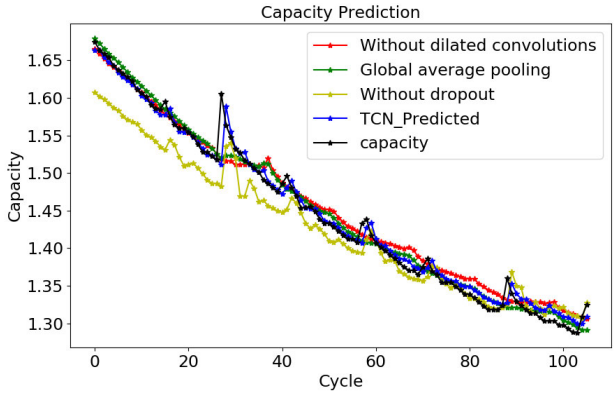

FIGURE 9. Comparison of results from different architectures.

values until all the test set data are predicted. The selection of model parameters is mostly obtained by the control variable method, which is also the most commonly used method for neural network to determine the optimal parameters. That means we can only change one parameter at a time to tune the model. Taking RMSE, MAE, and training time as criteria, a TCN model structure suitable for the data in this paper was selected after many experiments. To make the results more obvious, the basic parameters of the model used are configured as follows:

Number of iterations: 1000
Mini batch size: 128;
Size of the kernel: 3×1;
number of convolution kernels:256
Dilation factor: [1, 2, 4, 8, 16, 32, 64];
Optimizer: adam.

The comparison results are shown in Table 3. It is not difficult to see from the table that using skip connect will greatly improve the training speed of deep networks, compared with 11s faster without skip connect. In addition, dropout used by the model does not use the commonly used 0.5. For the experiments on this dataset, 0.2 has better accuracy, which means that 80% of the neurons are retained in each layer of the network. In contrast, the prediction accuracy of the

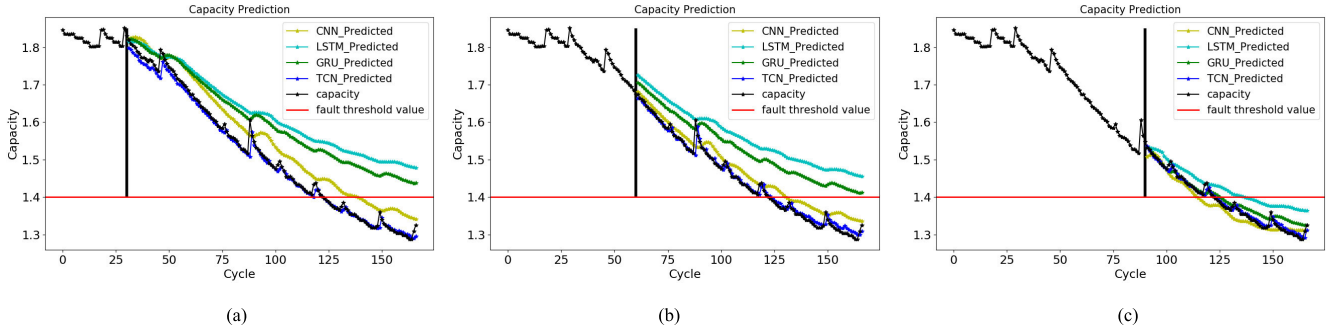

FIGURE 10. SOH monitoring of B0005. (a) Start at 30-th cycle. (b) Start at 60-th cycle. (c) Start at 90-th cycle.

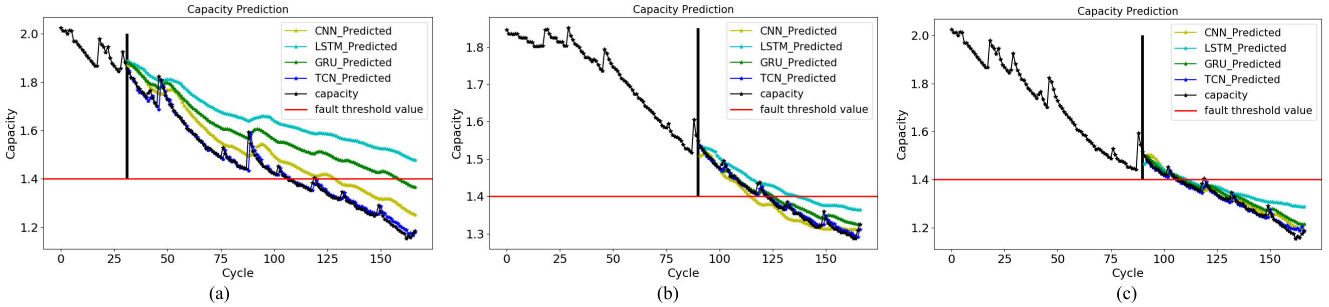

FIGURE 11. SOH monitoring of B0006. (a) Start at 30-th cycle. (b) Start at 60-th cycle. (c) Start at 90-th cycle.

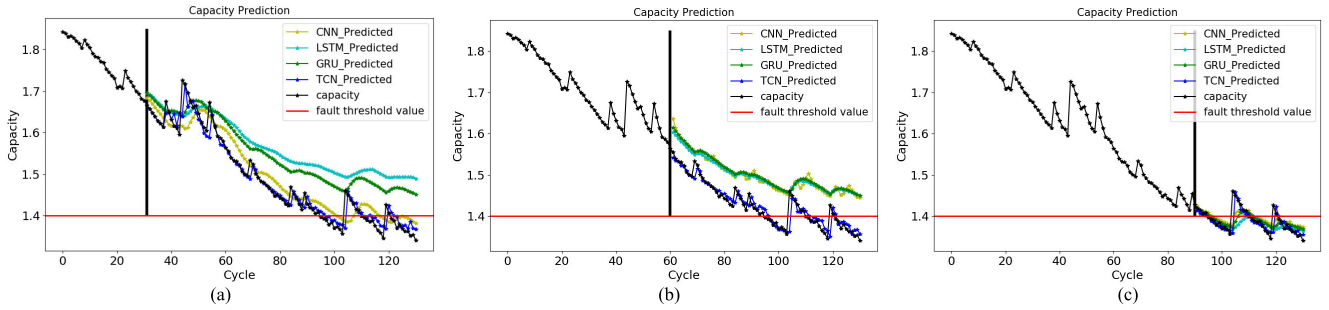

FIGURE 12. SOH monitoring of B0018. (a) Start at 30-th cycle. (b) Start at 60-th cycle. (c) Start at 90-th cycle.

TABLE 3. Comparison of model structure.

Model	RMSE	MAE	Training time(s)
TCN	0.013	0.008	33
Without skip connect	0.014	0.009	44
Without dropout	0.032	0.024	34
Without dilated convolution	0.018	0.014	33
Global average pooling	0.015	0.010	37

network without dropout is poor, and the model is overfitting. There is no obvious speed increase in the dataset by dilated convolutions, but expanding the receptive field allows more information to be integrated at less cost. In particular, the battery capacity sequence we deal with is multi-scale sequence, which can capture multi-scale information by using dilated convolutions to better capture local regeneration phenomena. As shown in Figure 9, the model that does not use dilated convolution is not sensitive to local regeneration phenomenon, and the prediction curve tends to be smooth, resulting in low overall prediction accuracy. The table also compares the global average pooling (GAP) used in many CNN models [41]. GAP is mainly used to solve the problem of overfitting caused by too many parameters in the fully connected layer, and it performs well in many classification and regression scenarios. For the capacity series, GAP can well predict the overall degradation trend, but the performance of local fluctuation prediction is worse than the fully connected layer, so the model still uses the fully connected layer for prediction.

B. VALIDATION OF SOH MONITORING PERFORMANCE

Effective monitoring of SOH means that the model has a small error in predicting the next SOH value, thus laying a foundation for RUL prediction. In addition, the earlier SOH is effectively estimated, the better the battery can be maintained in advance. Therefore, SOH monitoring is conducted from the 30th cycle in order to be closer to the actual

TABLE 4. SOH monitoring performance comparison.

Battery	Start point	Method	RMSE	MAE
B0005	30	LSTM	0.123	0.111
		GRU	0.101	0.092
		CNN	0.048	0.046
		TCN	0.014	0.009
	60	LSTM	0.120	0.114
		GRU	0.087	0.083
		CNN	0.031	0.028
		TCN	0.013	0.008
	90	LSTM	0.044	0.040
		GRU	0.019	0.015
		CNN	0.020	0.015
		TCN	0.008	0.006
B0006	30	LSTM	0.212	0.197
		GRU	0.138	0.129
		CNN	0.070	0.066
		TCN	0.020	0.012
	60	LSTM	0.153	0.145
		GRU	0.114	0.110
		CNN	0.067	0.063
		TCN	0.018	0.010
	90	LSTM	0.055	0.043
		GRU	0.027	0.023
		CNN	0.023	0.019
		TCN	0.014	0.009
B0018	30	LSTM	0.091	0.082
		GRU	0.071	0.066
		CNN	0.034	0.029
		TCN	0.020	0.014
	60	LSTM	0.075	0.071
		GRU	0.078	0.075
		CNN	0.076	0.072
		TCN	0.019	0.009
	90	LSTM	0.026	0.016
		GRU	0.023	0.015
		CNN	0.022	0.017
		TCN	0.019	0.009

usage. In addition, SOH monitoring results at different starting points were analyzed to better verify the accuracy and robustness of the model in SOH prediction. The prediction capabilities of the TCN model for the three different batteries under the 30th cycle, the 60th cycle, and the 90th cycle are analyzed in Table 4 and compared with the current commonly used methods. In order to accurately compare the performance of the model, LSTM model, GRU model and CNN model all have two hidden layers. During the prediction process, the parameter structure of the model is not changed and the optimal value is obtained through multiple experiments.

From Table 3, we can see that the model is not affected by the predicted starting point. For deep networks, the prediction accuracy will be higher when there is more training data. Figure 10, 11, and 12 are visualizations of battery cells B0005, B0006, and B0018 under different models and at different

TABLE 5. Comparison of RUL prediction results for B0005 batteries.

Method	RMSE	MAE	RUL_{Error}	$RUL_{prediction}$
	30cycle	RUL_{True}=94		
LSTM	0.029	0.023	13	107
GRU	0.027	0.023	13	107
CNN	0.037	0.033	14	108
TCN	0.030	0.027	5	99
	60cycle	RUL_{True}=64		
LSTM	0.027	0.024	11	75
GRU	0.029	0.025	12	76
CNN	0.044	0.042	14	78
TCN	0.018	0.014	2	66
	90cycle	RUL_{True}=34		
LSTM	0.024	0.021	6	40
GRU	0.019	0.016	4	38
CNN	0.036	0.034	11	45
TCN	0.009	0.007	0	34

starting points. Figure 10, 11, and 12 also show that the TCN model better fits the overall degradation trend of the capacity series than the currently used models, and effectively captures the local regeneration phenomena.

C. VALIDATION OF RUL PREDICTION PERFORMANCE

This section is mainly to verify the performance of the TCN model in RUL prediction compared with other models in the presence of offline data. Accurate prediction of RUL is the key to ensure timely battery replacement and system stability and safety. In this paper, EMD technology is used to reduce the prediction error caused by local fluctuations. The res of battery B0006 and B0018 after EMD denoising are used as offline training data, and battery B0005 with 168 cycles is used as test data. Different starting points are set and compared with different models to verify the accuracy of the TCN model. In the actual prediction process, the trained model is fine-tuned by combining some of the online data already given in order to improve the prediction accuracy of the model. The experimental results are the optimal values obtained from multiple experiments. From Table 5, we can find that the CNN model does not perform as well as the LSTM model in terms of RUL prediction. As an improved model of CNN, TCN model is not the best in terms of overall prediction accuracy in the early stage, but it always has the best effect in terms of RUL prediction. Moreover, the closer the starting point of the prediction is to the failure point, the more accurate the prediction result will be. In practical application, the accurate prediction of RUL in the later period is more important than the accurate prediction of RUL in the earlier period. In particular, the prediction accuracy of the TCN model for RUL in the 90th cycle can reach 0,

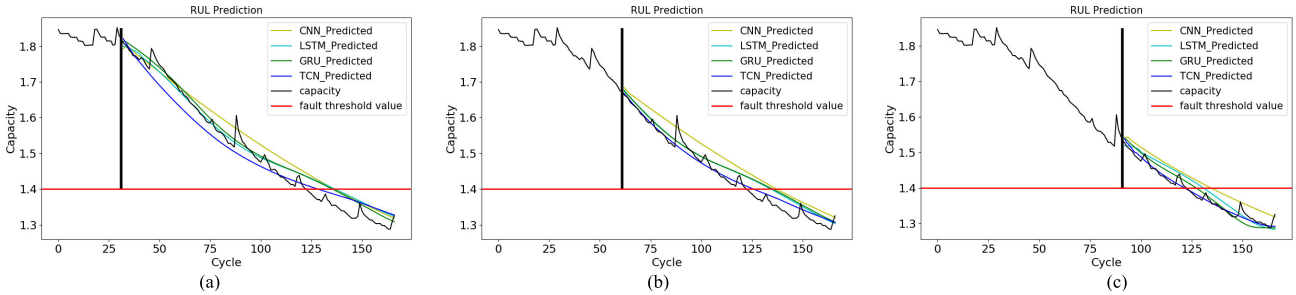

FIGURE 13. RUL prediction of B0005. (a) Start at 30-th cycle. (b) Start at 60-th cycle. (c) Start at 90-th cycle.

TABLE 6. Comparison of RUL prediction results for B0006 batteries.

Method	RMSE	MAE	RUL_{Error}	$RUL_{prediction}$
	30cycle	RUL_{True}=78		
LSTM	0.073	0.063	14	64
GRU	0.060	0.048	7	85
CNN	0.100	0.079	20	58
TCN	0.048	0.042	2	76
	60cycle	RUL_{True}=48		
LSTM	0.066	0.048	1	49
GRU	0.040	0.035	7	55
CNN	0.075	0.065	15	33
TCN	0.034	0.028	4	44
	90cycle	RUL_{True}=18		
LSTM	0.049	0.044	8	26
GRU	0.040	0.038	9	27
CNN	0.046	0.038	3	15
TCN	0.029	0.023	0	18

TABLE 7. Comparison of RUL prediction results for B0018 batteries.

Method	RMSE	MAE	RUL_{Error}	$RUL_{prediction}$
	30cycle	RUL_{True}=66		
LSTM	0.075	0.065	21	45
GRU	0.055	0.044	12	54
CNN	0.065	0.057	18	48
TCN	0.042	0.029	8	72
	60cycle	RUL_{True}=36		
LSTM	0.062	0.057	34	70
GRU	0.039	0.034	17	53
CNN	0.035	0.031	6	42
TCN	0.024	0.019	1	37
	90cycle	RUL_{True}=6		
LSTM	0.030	0.025	3	10
GRU	0.038	0.031	1	7
CNN	0.035	0.029	1	7
TCN	0.028	0.022	2	9

indicating the excellent performance of the TCN model in RUL prediction. In Figure 13, we can also find that the TCN model almost completely matches the degradation trend of volume sequence at the 90-th cycle. The RUL prediction for B0006 and B0018 is the same principle. We also present the predicted results for the two types of batteries as shown in figure 14 and figure 15. Table 6 and table 7 show the comparison of prediction accuracy. From the perspective of the effective prediction of lithium batteries with three different degradation trends, our model can realize the RUL prediction of lithium batteries with high efficiency and stability.

D. VERIFY THE RELIABILITY OF THE MODEL

In this section, to verify the reliability of the model, experimental analysis is conducted on battery cells with CS2 discharge current of 0.5C and 1C, that is, the model is also verified to have good prediction accuracy in the case of more cycles. The starting point is selected as the middle position so as to evaluate the prediction accuracy of the model more

TABLE 8. SOH monitoring under different discharge current.

Battery cell	Discharge current	RMSE	MAE
CS2_34	0.5C	0.011	0.009
CS2_35	0.5C	0.011	0.010
CS2_37	1C	0.009	0.008

reasonably. The SOH and RUL of the battery cell are predicted from the 360th cycle. The monitoring results of SOH are given in Table 8. From the perspective of RMSE and MAE, the model also achieves high prediction accuracy under different working conditions. We can also find this point from Figure 16. Combining online data to make a single-step prediction model can capture local fluctuations while fitting the overall trend.

The predicted results of RUL are given in Table 9. After EMD de-noising, the data is taken as the input of the model, and the data of two battery cells are taken as offline data for training, while the other data is taken as the prediction.

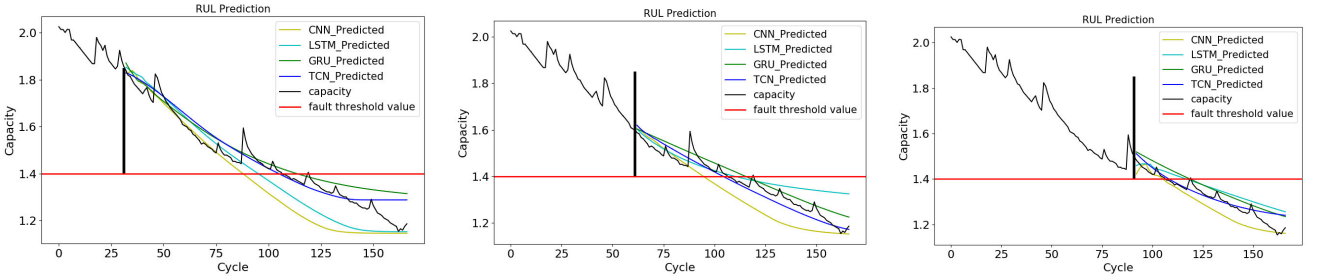

FIGURE 14. RUL prediction of B0006. (a) Start at 30-th cycle. (b) Start at 60-th cycle. (c) Start at 90-th cycle.

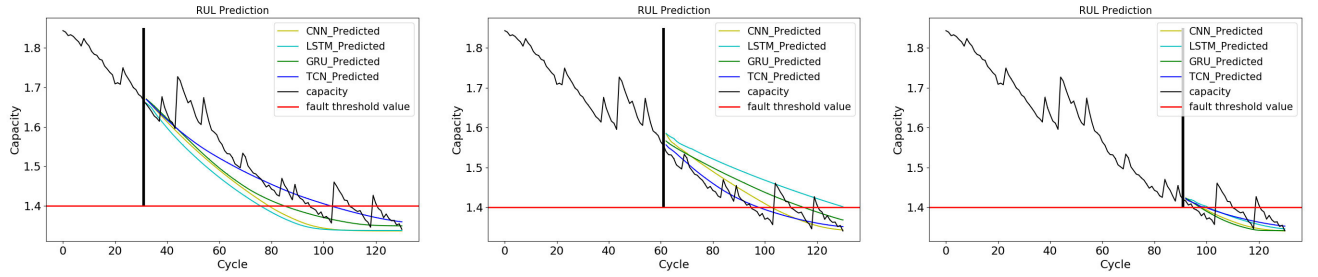

FIGURE 15. RUL prediction of B0018. (a) Start at 30-th cycle. (b) Start at 60-th cycle. (c) Start at 90-th cycle.

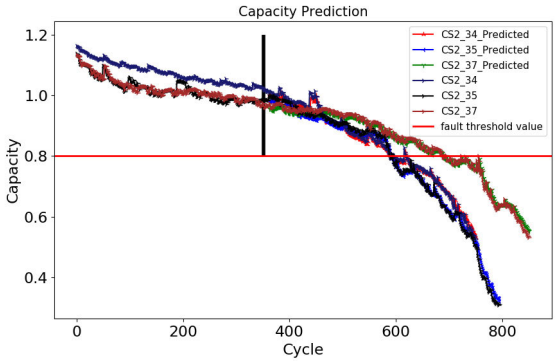

FIGURE 16. SOH monitoring under different working conditions.

TABLE 9. RUL prediction performance.

Battery cell	RMSE	MAE	RUL_{True}	$RUL_{prediction}$	RUL_{Error}
CS2_34	0.018	0.014	244	255	6
CS2_35	0.020	0.010	235	238	3

This paper only gives the prediction results of two kinds of battery cells, because CS_37 is inconsistent with the discharge conditions of the other two batteries. If there are enough training data of different conditions, it can also be predicted accurately. As can be seen from Figure 17, although the offline training data is limited, the model can also be predicted accurately after some online data are fine-tuned.

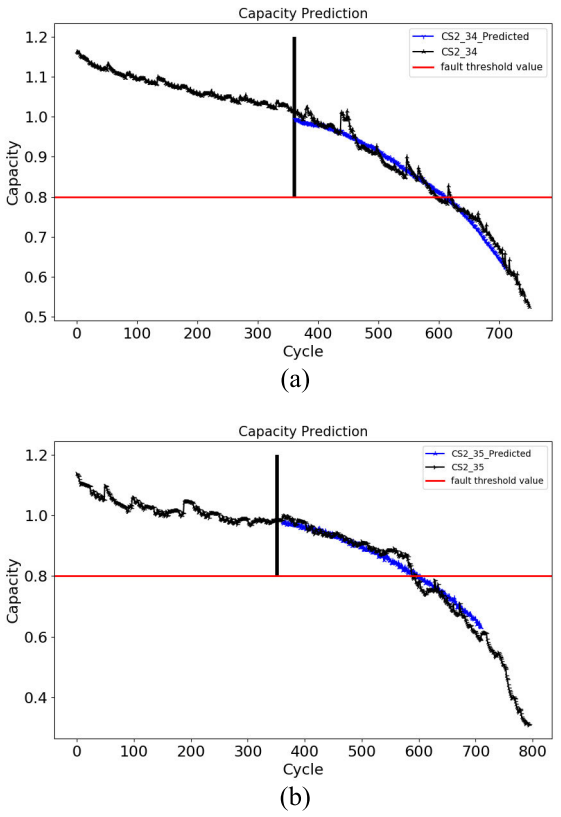

FIGURE 17. RUL prediction. (a) RUL prediction of CS2_34. (b) RUL prediction of CS2_35.

V. CONCLUSION

In recent years, the prognostic and health management (PHM) of lithium-ion batteries has received increasing attention. SOH monitoring and RUL prediction is a key technology in PHM. Effective SOH monitoring is conducive to prolonging battery life, while accurate RUL prediction is an essential means to ensure system security. Therefore, we need to take measures to make effective predictions for both.

In this paper, we propose a TCN model suitable for SOH monitoring and RUL prediction. Dilated convolution and residual connection techniques that perform well in other

fields are used to increase the model's sensitivity to local regeneration phenomenon. It solves the problem that the overall prediction accuracy of the traditional network model due to the local regeneration phenomenon is not high, and other methods need to be combined to complicate the SOH monitoring process. At the same time, this study aims at the recent phenomenon that LSTM model and GRU model are the main methods in SOH monitoring and RUL prediction of lithium-ion batteries. The TCN model is used for the first time to complete the prediction task of lithium batteries, and the monitoring of SOH of lithium batteries and the prediction ability of RUL of lithium batteries are verified by the TCN model, thus providing a new improved route for the prediction task of lithium-ion batteries.

Through a large number of experiments and comparisons on two commonly used lithium battery dataset, we find that the proposed model can well monitor SOH with online data and accurately capture local regeneration phenomenon. Compared with the problems of traditional networks that are greatly affected by the starting point, on the NASA dataset, the average RMSE accuracy of the TCN model is about 5% higher than that of the traditional network at different starting points. For the RUL prediction task, in the case of offline data, the offline data can be de-noised by EMD and then combined with some online data to fine-tune the model to achieve high-precision RUL prediction. Compared with other models, the average RUL_{Error} is nearly 8 cycles higher. Therefore, compared with LSTM, GRU, and CNN models, TCN model has the characteristics of less influence from the starting point, higher prediction accuracy and stronger robustness.

ACKNOWLEDGMENT

Thanks to all authors for their help in improving this research.

REFERENCES

[1] M. A. Hannan, M. S. H. Lipu, A. Hussain, and A. Mohamed, "A review of lithium-ion battery state of charge estimation and management system in electric vehicle applications: Challenges and recommendations," *Renew. Sustain. Energy Rev.*, vol. 78, pp. 834–854, Oct. 2017.

[2] Y. Li, K. Liu, A. M. Foley, A. Zülke, M. Berecibar, E. Nanini-Maury, J. Van Mierlo, and H. E. Hoster, "Data-driven health estimation and lifetime prediction of lithium-ion batteries: A review," *Renew. Sustain. Energy Rev.*, vol. 113, Oct. 2019, Art. no. 109254.

[3] M. Huang, M. Kumar, C. Yang, and A. Soderlund, "Aging estimation of lithium-ion battery cell using an electrochemical model-based extended Kalman filter," in *Proc. AIAA Scitech Forum*, Jan. 2019, p. 0785.

[4] R. Xiong, L. Li, Z. Li, Q. Yu, and H. Mu, "An electrochemical model based degradation state identification method of lithium-ion battery for all-climate electric vehicles application," *Appl. Energy*, vol. 219, pp. 264–275, Jun. 2018.

[5] L. De Sutter, Y. Firouz, J. De Hoog, N. Omar, and J. Van Mierlo, "Battery aging assessment and parametric study of lithium-ion batteries by means of a fractional differential model," *Electrochimica Acta*, vol. 305, pp. 24–36, May 2019.

[6] R. Ahmed, J. Gazzarri, S. Onori, S. Habibi, R. Jackey, K. Rzemien, J. Tjong, and J. LeSage, "Model-based parameter identification of healthy and aged li-ion batteries for electric vehicle applications," *SAE Int. J. Alternative Powertrains*, vol. 4, no. 2, pp. 233–247, 2015.

[7] S. Torai, M. Nakagomi, S. Yoshitake, S. Yamaguchi, and N. Oyama, "State-of-health estimation of $LiFePO_4$/graphite batteries based on a model using differential capacity," *J. Power Sour.*, vol. 306, pp. 62–69, Feb. 2016.

[8] C. Lyu, Y. Song, J. Zheng, W. Luo, G. Hinds, J. Li, and L. Wang, "*In situ* monitoring of lithium-ion battery degradation using an electrochemical model," *Appl. Energy*, vol. 250, pp. 685–696, Sep. 2019.

[9] J. Yang, B. Xia, W. Huang, Y. Fu, and C. Mi, "Online state-of-health estimation for lithium-ion batteries using constant-voltage charging current analysis," *Appl. Energy*, vol. 212, pp. 1589–1600, Feb. 2018.

[10] Y. Cui, P. Zuo, C. Du, Y. Gao, J. Yang, X. Cheng, Y. Ma, and G. Yin, "State of health diagnosis model for lithium ion batteries based on real-time impedance and open circuit voltage parameters identification method," *Energy*, vol. 144, pp. 647–656, Feb. 2018.

[11] S. Shen, M. K. Sadoughi, X. Chen, M. Hong, and C. Hu, "Online estimation of lithium-ion battery capacity using deep convolutional neural networks," in *Proc. 44th Design Autom. Conf.*, vol. 2A, Aug. 2018, pp. 1–8.

[12] Y. Choi, S. Ryu, K. Park, and H. Kim, "Machine learning-based lithium-ion battery capacity estimation exploiting multi-channel charging profiles," *IEEE Access*, vol. 7, pp. 75143–75152, 2019.

[13] D. Yang, X. Zhang, R. Pan, Y. Wang, and Z. Chen, "A novel Gaussian process regression model for state-of-health estimation of lithium-ion battery using charging curve," *J. Power Sour.*, vol. 384, pp. 387–395, Apr. 2018.

[14] P. Guo, Z. Cheng, and L. Yang, "A data-driven remaining capacity estimation approach for lithium-ion batteries based on charging health feature extraction," *J. Power Sour.*, vol. 412, pp. 442–450, Feb. 2019.

[15] D. M. E. Orchard, L. Tang, B. Saha, K. Goebel, and D. G. J. Vachtsevanos, "Risk-sensitive Particle-Filtering-based prognosis framework for estimation of remaining useful life in energy storage devices," *Stud. Inform. Control*, vol. 19, no. 3, pp. 209–218, Sep. 2010.

[16] J. Yu, "State of health prediction of lithium-ion batteries: Multiscale logic regression and Gaussian process regression ensemble," *Rel. Eng. Syst. Saf.*, vol. 174, pp. 82–95, Jun. 2018.

[17] X. Pang, R. Huang, J. Wen, Y. Shi, J. Jia, and J. Zeng, "A lithium-ion battery RUL prediction method considering the capacity regeneration phenomenon," *Energies*, vol. 12, no. 12, p. 2247, 2019.

[18] T. Sun, B. Xia, Y. Liu, Y. Lai, W. Zheng, H. Wang, W. Wang, and M. Wang, "A novel hybrid prognostic approach for remaining useful life estimation of lithium-ion batteries," *Energies*, vol. 12, no. 19, p. 3678, 2019.

[19] L. Jayasinghe, T. Samarasinghe, C. Yuen, J. C. N. Low, and S. S. Ge, "Temporal convolutional memory networks for remaining useful life estimation of industrial machinery," 2018, *arXiv:1810.05644*. [Online]. Available: http://arxiv.org/abs/1810.05644

[20] A. Z. Hinchi and M. Tkiouat, "Rolling element bearing remaining useful life estimation based on a convolutional long-short-term memory network," *Procedia Comput. Sci.*, vol. 127, pp. 123–132, 2018.

[21] X. Li, L. Zhang, Z. Wang, and P. Dong, "Remaining useful life prediction for lithium-ion batteries based on a hybrid model combining the long short-term memory and Elman neural networks," *J. Energy Storage*, vol. 21, pp. 510–518, Feb. 2019.

[22] F. Yang, W. Li, C. Li, and Q. Miao, "State-of-charge estimation of lithium-ion batteries based on gated recurrent neural network," *Energy*, vol. 175, pp. 66–75, May 2019.

[23] Y. Zhang, R. Xiong, H. He, and M. G. Pecht, "Long short-term memory recurrent neural network for remaining useful life prediction of lithium-ion batteries," *IEEE Trans. Veh. Technol.*, vol. 67, no. 7, pp. 5695–5705, Jul. 2018.

[24] B. Xiao, Y. Liu, and B. Xiao, "Accurate state-of-charge estimation approach for lithium-ion batteries by gated recurrent unit with ensemble optimizer," *IEEE Access*, vol. 7, pp. 54192–54202, 2019.

[25] Y. Zhou, Y. Huang, J. Pang, and K. Wang, "Remaining useful life prediction for supercapacitor based on long short-term memory neural network," *J. Power Sour.*, vol. 440, Nov. 2019, Art. no. 227149.

[26] J. Qu, F. Liu, Y. Ma, and J. Fan, "A neural-network-based method for RUL prediction and SOH monitoring of lithium-ion battery," *IEEE Access*, vol. 7, pp. 87178–87191, 2019.

[27] F. Karim, S. Majumdar, H. Darabi, and S. Harford, "Multivariate LSTM-FCNs for time series classification," *Neural Netw.*, vol. 116, pp. 237–245, Aug. 2019.

[28] H. Dong, X. Jin, Y. Lou, and C. Wang, "Lithium-ion battery state of health monitoring and remaining useful life prediction based on support vector regression-particle filter," *J. Power Sour.*, vol. 271, pp. 114–123, Dec. 2014.

[29] B. Saha, K. Goebel, S. Poll, and J. Christophersen, "Prognostics methods for battery health monitoring using a Bayesian framework," *IEEE Trans. Instrum. Meas.*, vol. 58, no. 2, pp. 291–296, Feb. 2009.
[30] Y. Xing, E. W. M. Ma, K.-L. Tsui, and M. Pecht, "An ensemble model for predicting the remaining useful performance of lithium-ion batteries," *Microelectron. Rel.*, vol. 53, no. 6, pp. 811–820, Jun. 2013.
[31] K. A. Severson, P. M. Attia, N. Jin, N. Perkins, B. Jiang, Z. Yang, M. H. Chen, M. Aykol, P. K. Herring, D. Fraggedakis, M. Z. Bazant, S. J. Harris, W. C. Chueh, and R. D. Braatz, "Data-driven prediction of battery cycle life before capacity degradation," *Nature Energy*, vol. 4, no. 5, pp. 383–391, May 2019.
[32] S. Bai, J. Zico Kolter, and V. Koltun, "An empirical evaluation of generic convolutional and recurrent networks for sequence modeling," 2018, *arXiv:1803.01271*. [Online]. Available: http://arxiv.org/abs/1803.01271
[33] A. van den Oord, S. Dieleman, H. Zen, K. Simonyan, O. Vinyals, A. Graves, N. Kalchbrenner, A. Senior, and K. Kavukcuoglu, "WaveNet: A generative model for raw audio," 2016, *arXiv:1609.03499*. [Online]. Available: http://arxiv.org/abs/1609.03499
[34] F. Yu and V. Koltun, "Multi-scale context aggregation by dilated convolutions," 2015, *arXiv:1511.07122*. [Online]. Available: http://arxiv.org/abs/1511.07122
[35] P. Wang, P. Chen, Y. Yuan, D. Liu, Z. Huang, X. Hou, and G. Cottrell, "Understanding convolution for semantic segmentation," in *Proc. IEEE Winter Conf. Appl. Comput. Vis. (WACV)*, Mar. 2018, pp. 1451–1460.
[36] L.-C. Chen, G. Papandreou, I. Kokkinos, K. Murphy, and A. L. Yuille, "DeepLab: Semantic image segmentation with deep convolutional nets, atrous convolution, and fully connected CRFs," *IEEE Trans. Pattern Anal. Mach. Intell.*, vol. 40, no. 4, pp. 834–848, Apr. 2018.
[37] K. He, X. Zhang, S. Ren, and J. Sun, "Deep residual learning for image recognition," in *Proc. IEEE Conf. Comput. Vis. Pattern Recognit. (CVPR)*, Jun. 2016, pp. 770–778.
[38] N. Srivastava, G. Hinton, and A. Krizhevsky, "Dropout: A simple way to prevent neural networks from overfitting," *J. Mach. Learn. Res.*, vol. 15, no. 1, pp. 1929–1958, 2014.
[39] N. E. Huang, Z. Shen, S. R. Long, M. C. Wu, H. H. Shih, Q. Zheng, N.-C. Yen, C. C. Tung, and H. H. Liu, "The empirical mode decomposition and the Hilbert spectrum for nonlinear and non-stationary time series analysis," *Proc. Roy. Soc. London. A, Math., Phys. Eng. Sci.*, vol. 454, no. 1971, pp. 903–995, Mar. 1998.
[40] M. E. Torres, M. A. Colominas, G. Schlotthauer, and P. Flandrin, "A complete ensemble empirical mode decomposition with adaptive noise," in *Proc. IEEE Int. Conf. Acoust., Speech Signal Process. (ICASSP)*, May 2011, pp. 4144–4147.
[41] M. Lin, Q. Chen, and S. Yan, "Network in network," 2013, *arXiv:1312.4400*. [Online]. Available: http://arxiv.org/abs/1312.4400

DANHUA ZHOU received the B.S. degree in automation in 2018. He is currently pursuing the M.S. degree in control science and engineering with Dalian Polytechnic University, Dalian, China. His research interests include prognostic and health management (PHM) and deep learning.

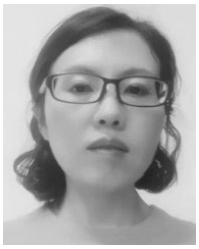

ZHANYING LI was born in 1979. She received the Ph.D. degree in pattern recognition and intelligent systems from Harbin Engineering University, Heilongjiang, China, in 2012. She is currently an Associate Professor at the School of Information Science and Engineering, Dalian Polytechnic University, Dalian, China. Her research interests include intelligent control, neural networks, and time series prediction.

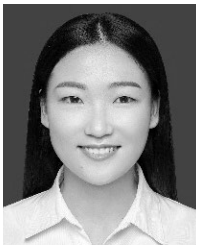

JIALI ZHU received the B.S. degree in automation in 2018. She is currently pursuing the M.S. degree in control science and engineering with the University of Shanghai for Science and Technology, Shanghai, China. Her research interests include image segmentation and deep learning.

HAICHUAN ZHANG received the Ph.D. degree in mechanical and electrical engineering from the Dalian University of Technology, Dalian, China, in 2011. His main research interests include intelligent control and mechatronics. He is currently an Associate Professor with the School of Information Science and Engineering, Dalian Polytechnic University, Dalian. In recent years, he has undertaken a number of national natural science foundation projects, provincial projects, and enterprise cooperation projects.

LIN HOU received the B.S. degree in automation in 2017. She is currently pursuing the M.S. degree in control science and engineering with Dalian Polytechnic University, Dalian, China. Her research interests include image processing and systems control.